Supplementary Material

Exploiting oxidative coupling of methane performed over $La_2(Ce_{1-x}Mg_x)_2O_{7-\delta}$ catalysts with disordered defective cubic fluorite structure

Davi D. Petrolini[a], Francielle F. C. Marcos[b], Alessandra F. Lucrédio[a], Valmor R. Mastelaro[c], José M. Assaf[d], and Elisabete M. Assaf[a]*

[a]*University of São Paulo, São Carlos Institute of Chemistry, Av. Trabalhador São-Carlense, 400, São Carlos, SP, 13560-970, Brazil.*
[b]*University of São Paulo, Escola Politécnica of the University of São Paulo, Av. Prof. Luciano Gualberto, t. 3, 380, São Paulo, SP, 05508-010, Brazil*
[c]*University of São Paulo, São Carlos Institute of Physics, Av. Trabalhador São-Carlense, 400, São Carlos, SP, 13560-970, Brazil.*
[d]*Federal University of São Carlos, Rod. W. Luiz, km 235, São Carlos, SP, 13565-905, Brazil.*

$$X_{CH_4} = \frac{moles\ of\ methane\ reacted}{moles\ of\ methane\ in\ the\ feed} x\ 100\ (Eq.\ 1)$$

$$S_{C_2} = \frac{2(moles\ of\ ethane\ and\ ethylene\ formed)}{moles\ of\ methane\ reacted} x\ 100\ (Eq.\ 2)$$

$$Y_{C_2} = X_{CH_4} x S_{C_2} \div 100\ (Eq.\ 3)$$

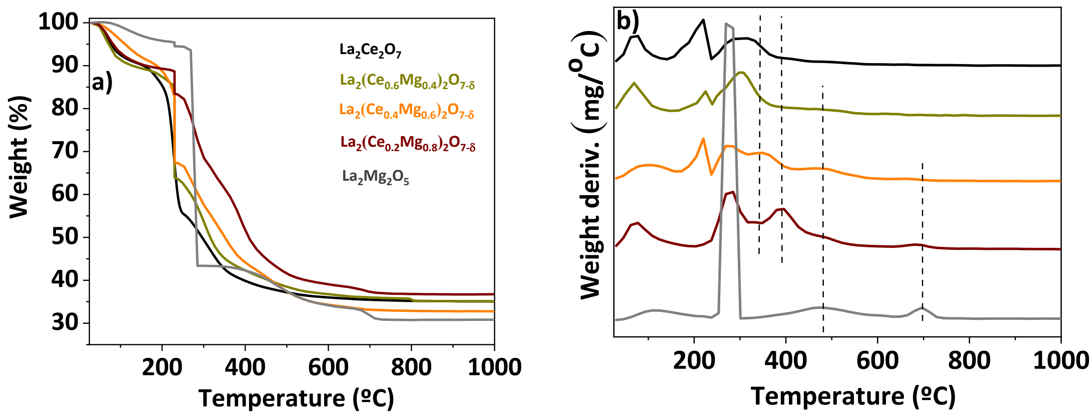

Figure 1S. a) Thermogravimetric and b) weight derivative curves of the as-synthesized $La_2(Ce_{1-x}Mg_x)_2O_{7-\delta}$ catalysts.

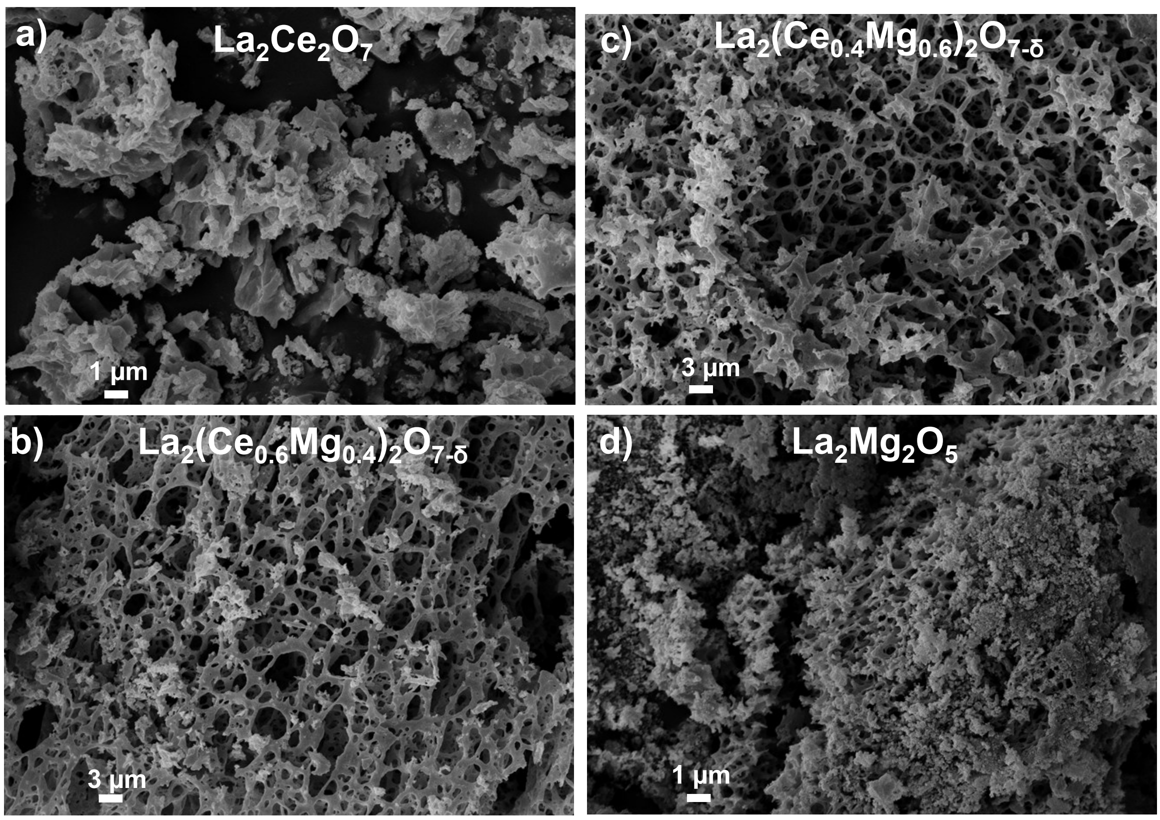

Figure 2S. Scanning electron microscopy images of the $La_2(Ce_{1-x}Mg_x)_2O_{7-\delta}$ catalysts.

$La_2Ce_2O_7$

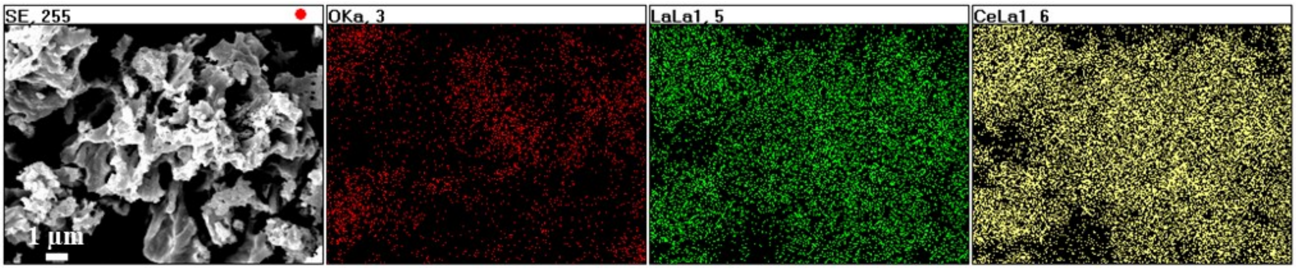

$La_2(Ce_{0.6}Mg_{0.4})_2O_{7-\delta}$

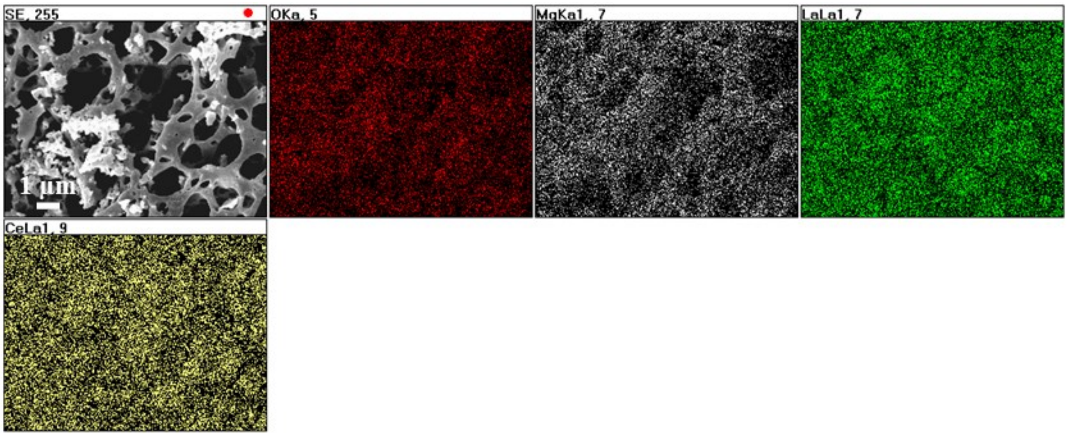

$La_2(Ce_{0.4}Mg_{0.6})_2O_{7-\delta}$

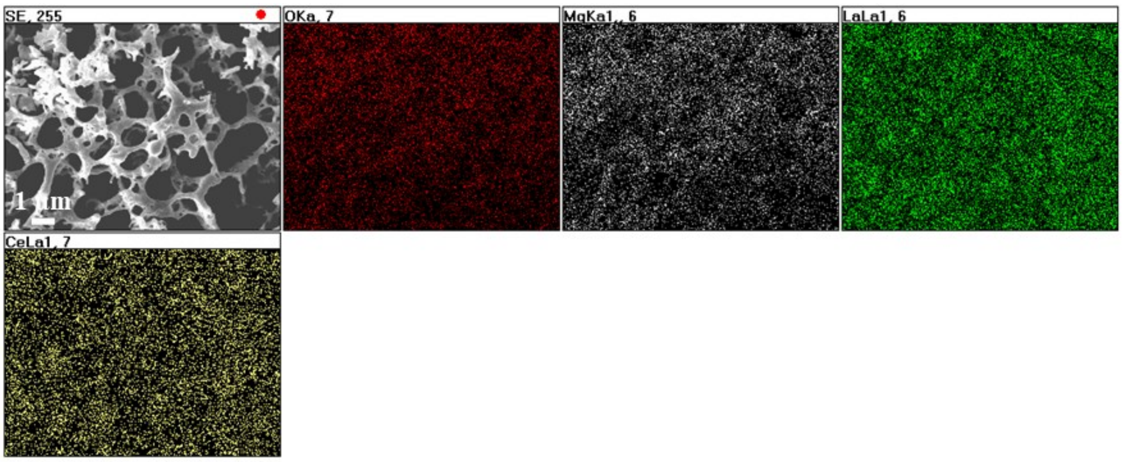

$La_2Mg_2O_5$

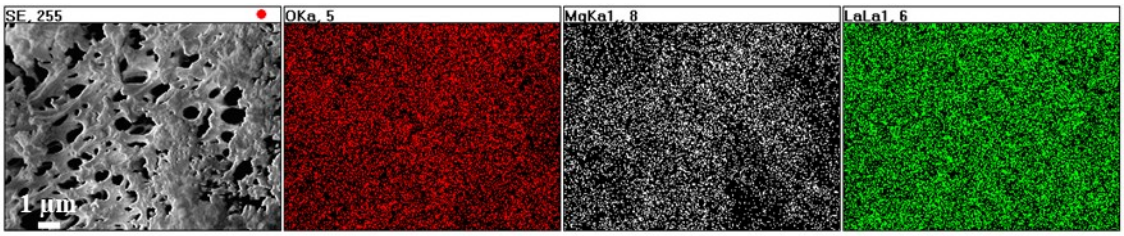

Figure 3S. SEM mapping images of the $La_2(Ce_{1-x}Mg_x)_2O_{7-\delta}$ catalysts.

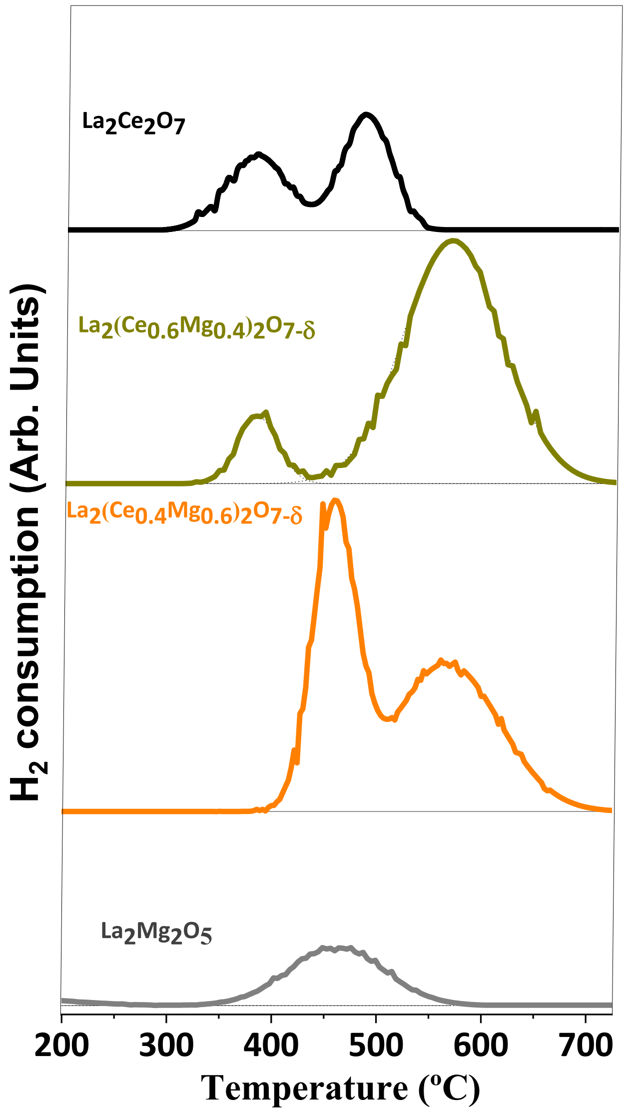

Figure 4S. TPR profiles of the $La_2(Ce_{1-x}Mg_x)_2O_{7-\delta}$ catalysts.

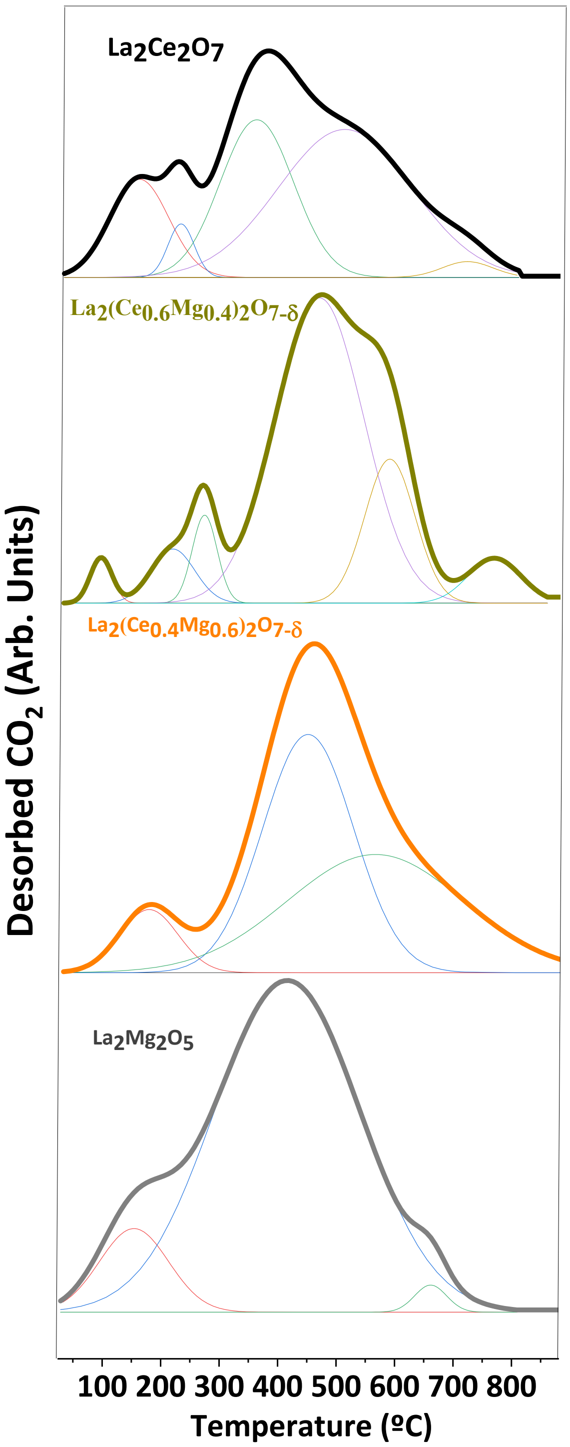

Figure 5S. CO_2-TPD profiles of the $La_2(Ce_{1-x}Mg_x)_2O_{7-\delta}$ catalysts.

Table 1S. Binding energies obtained by XPS for the surface elements of the $La_2(Ce_{1-x}Mg_x)_2O_{7-\delta}$ catalysts. The integrated areas of the cerium peaks are shown in parentheses.

Catalyst	**Binding energy (eV) Ce^{3+}**	**Binding energy (eV) Ce^{4+}**	**Binding energy (eV) La^{3+}**	**Binding energy (eV) O 1s**	**Binding energy (eV) C 1s**	**Binding energy (eV) Mg 2s**

$La_2Ce_2O_7$	881.6 (3594) 885.6 (2732) 896.7 (1040) 900.7 (982)	882.5 (9001) 888.4 (6200) 897.9 (7989) 900.5 (6366) 906.5 (4445) 916.1 (6629)	832.9 835.1 837.9 838.4 849.5 851.7 854.6 855.3	528.8 531.4 532.9	284.6 285.9 288.0 289.3	--------------
$La_2(Ce_{0.6}Mg_{0.4})_2O_{7-\delta}$	881.2 (6428) 885.2 (4286) 897.3 (590) 901.3 (393)	882.2 (4864) 888.2 (3242) 897.8 (6864) 900.7 (4184) 906.7 (2789) 916.1 (5349)	833.7 835.2 837.7 839.2 850.3 852.1 854.3 855.7	528.9 531.5 533.1	284.7 286.1 288.2 289.8	88.9
$La_2(Ce_{0.4}Mg_{0.6})_2O_{7-\delta}$	881.6 (2385) 885.6 (1684) 897.5 (893) 901.5 (740)	882.5 (5141) 888.5 (3921) 897.8 (5764) 903.7 (5274) 908.7 (3483) 916.1 (3715)	833.6 835.5 838.3 838.4 850.1 851.9 855.1 855.2	529.0 531.5 532.9	284.7 286.0 288.3 289.9	88.7
$La_2Mg_2O_5$	------------------------	------------------------	835.4 838.8 852.2 855.5	531.6 533.1	284.8 286.2 288.3 289.9	88.9

Table 2S. Analysis of the surface chemical compositions of the $La_2(Ce_{1-x}Mg_x)_2O_{7-\delta}$ catalysts.

Catalyst	**C (%)**	**O (%)**	**La (%)**	**Ce (%)**	**Mg (%)**
$La_2Ce_2O_7$	63.3	32.5	2.7	1.5	0.0
$La_2(Ce_{0.6}Mg_{0.4})_2O_{7-\delta}$	52.4	34.7	3.0	1.1	8.8
$La_2(Ce_{0.4}Mg_{0.6})_2O_{7-\delta}$	55.0	32.3	2.5	0.9	9.2
$La_2Mg_2O_5$	57.4	28.8	1.8	0.0	12.0

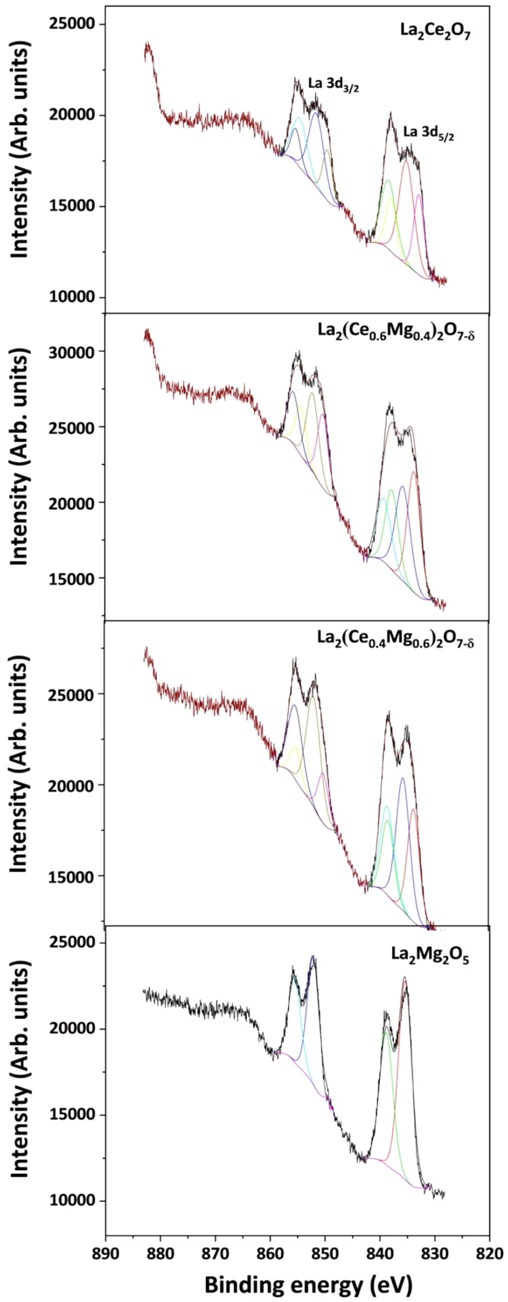

Figure 6S. La 3d spectra of the $La_2(Ce_{1-x}Mg_x)_2O_{7-\delta}$ catalysts.

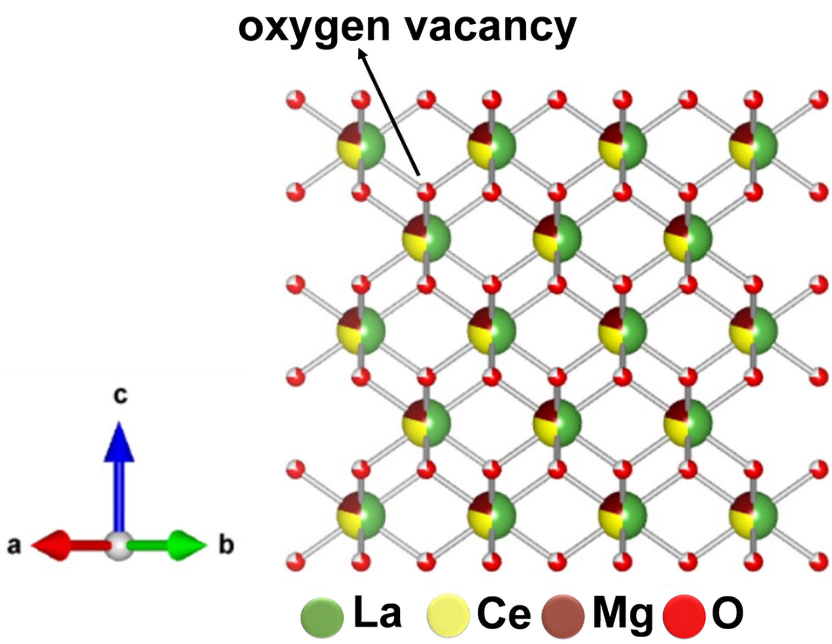

Figure 7S. Representation of the disordered defective cubic fluorite phase structure for the $La_2(Ce_{0.6}Mg_{0.4})_2O_{7-\delta}$ catalyst.

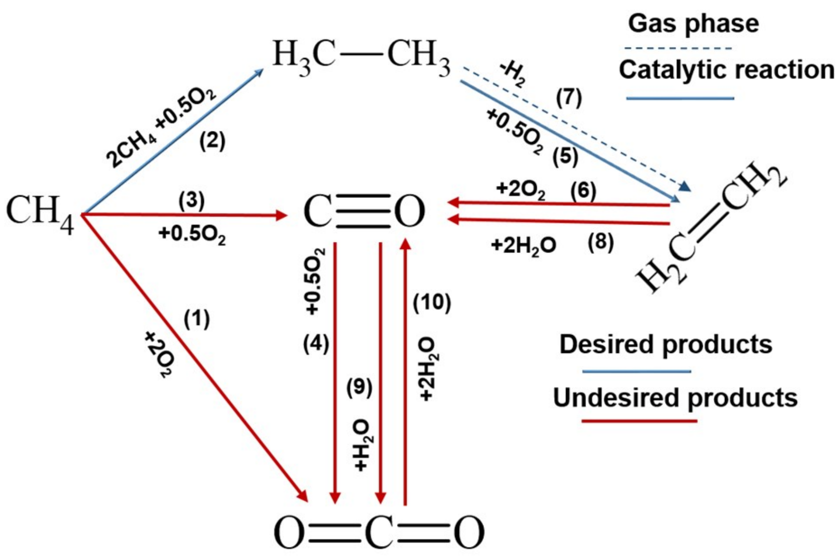

Scheme 1S. Major products and reaction pathways involved in the oxidative coupling of methane.

$$S_{CO_x} = \frac{moles\ of\ CO\ or\ CO_2\ formed}{moles\ of\ methane\ reacted} x\ 100\ (Eq.\ 2)$$

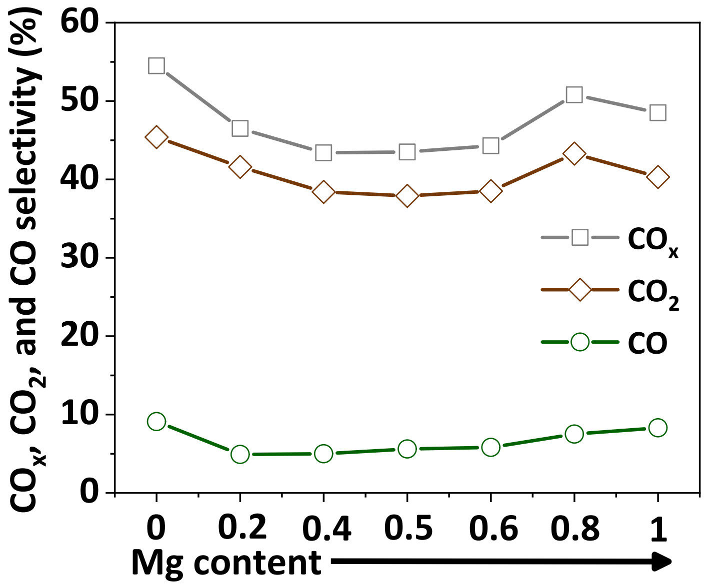

Figure 8S. CO_x (CO_2 + CO), CO_2, and CO selectivities in the OCM performed over the $La_2(Ce_{1-x}Mg_x)_2O_{7-\delta}$ catalysts with different Mg contents. Reaction conditions: 200 mg catalyst, CH_4:O_2:N_2 = 4:1:4, WHSV = 18,000 mL.h^{-1}.g$_{cat}^{-1}$, 800 ºC.

Table 3S. C_2 yields, O_2 conversions, and C_2, C_2H_4, C_2H_6, CO_2, and CO selectivities for the La_2O_3, MgO, and CeO_2 catalysts. Reaction conditions: 60 mL.min^{-1} of CH_4:O_2:N_2 = 4:1:4, WHSV = 18,000 mL.h^{-1}.g$_{cat}^{-1}$, 800 ºC.

Catalyst	C_2 yield (%)	C_2 selectivity (%)	C_2H_4 selectivity (%)	C_2H_6 selectivity (%)	CO_2 selectivity (%)	CO selectivity (%)	O_2 conversion (%)
La_2O_3	7.8	55.8	32.5	23.3	36.1	8.2	100
MgO	7.0	46.7	30.3	16.4	27.6	25.7	85
CeO_2	0.9	7.0	3.8	3.2	72.7	20.3	100

Table 4S. Performances (conversions and C_2 selectivities or yields) and reaction conditions for catalysts reported in the literature for the OCM reaction.

Catalyst	Reaction condition	Conversion (%)	Selectivity (S) or yield (Y) for C_2 (%)	Ref.
Mn_xO_y-Na_2WO_4/COK-12 (ordered mesoporous silica)	775 ºC, 100 mg catalyst, CH_4/O_2 = 4	24	60 (S)	[1]
Li/Sm_2O_3/MgO	700 ºC, 0.4 g catalyst, 2400 h^{-1}, CH_4/O_2 = 4	24	64 (S)	[2]
Sm_2O_3/MgO	700 ºC, 0.4 g catalyst, 2400 h^{-1}, CH_4/O_2 = 4	22	52 (S)	[2]
Mn_xO_y-Na_2WO_4 supported over SBA-15	750 ºC, 50 mg catalyst, CH_4/O_2 = 4	14	70 (S)	[3]
Mn_xO_y-Na_2WO_4/La_2O_3	750 ºC, 50 mg catalyst, CH_4/O_2 = 4	18	34 (S)	[3]
Mn_xO_y-Na_2WO_4/CaO	750 ºC, 50 mg catalyst, CH_4/O_2 = 4	18	26 (S)	[3]

Mn_xO_y-Na_2WO_4/SrO	750 ºC, 50 mg catalyst, CH_4/O_2 = 4	5.4	25 (S)	[3]
Mn_xO_y-Na_2WO_4/Al_2O_3	750 ºC, 50 mg catalyst, CH_4/O_2 = 4	13	25 (S)	[3]
Mn_xO_y-Na_2WO_4/ZrO_2	750 ºC, 50 mg catalyst, CH_4/O_2 = 4	10	21 (S)	[3]
Mn_xO_y-Na_2WO_4/Fe_2O_3	750 ºC, 50 mg catalyst, CH_4/O_2 = 4	2.3	73 (S)	[3]
Mn_xO_y-Na_2WO_4/Fe_3O_4	750 ºC, 50 mg catalyst, CH_4/O_2 = 4	1.6	63 (S)	[3]
Mn_xO_y-Na_2WO_4/TiO_2-rutile	750 ºC, 50 mg catalyst, CH_4/O_2 = 4	3.6	79 (S)	[3]
Mn_xO_y-Na_2WO_4/TiO_2- anatase	750 ºC, 50 mg catalyst, CH_4/O_2 = 4	1.6	63 (S)	[3]
Cs/Sr/MgO	794 ºC, 1 g catalyst, CH_4/O_2 = 3	33	59 (S)	[4]
Cs/Ba/MgO	820 ºC, 1 g catalyst, CH_4/O_2 = 3	32	57 (S)	[4]
1 wt.% Li/MgO	800 ºC, 4500 h^{-1}, CH_4/O_2 = 2	38	35 (S)	[5]
CaO/ZnO, Ca/Zn = 1.3	800 ºC, 4500 h^{-1}, CH_4/O_2 = 2	36	30 (S)	[5]
Na_2WO_4/Mn/SiO_2	850 ºC, 10,000 h^{-1}, CH_4/O_2 = 3.5	32	57 (S)	[6]
Na_2WO_4/Mn/SiO_2 modified with 16.7 wt.% MgO	850 ºC, 10,000 h^{-1}, CH_4/O_2 = 2	50	38 (S)	[6]
Na_2WO_4/Mn/SiO_2 modified with 40 wt.% TiO_2	850 ºC, 10,000 h^{-1}, CH_4/O_2 = 2	39	59 (S)	[6]
10% Na_2WO_4-5% Mn/SiO_2, modified with 5% La	800 ºC, 1 g of catalyst, 10% N_2, $CH_4:O_2$ = 32:8,	Not reported	24 (Y)	[7]
5 wt.% Ba/La_2O_3	150 ºC, 200 mg catalyst, 18 h^{-1}, (in electric field, 3.0 mA, 600 V)	6.3	32.3 (S)	[8]
Mn_xO_y-Na_2WO_4/SIC (porous)	800 ºC, 50 mg catalyst, CH_4/O_2 = 4	35	10 (S)	[9]
$La_2Ti_2O_7$	800 ºC, 200 mg catalyst, CH_4/O_2 = 4	~18	~35 (S)	[10]
$La_2Zr_2O_7$	800 ºC, 200 mg catalyst, CH_4/O_2 = 4	~24	~55 (S)	[10]
$La_2Ce_2O_7$	800 ºC, 200 mg catalyst, CH_4/O_2 = 4	~29	~59 (S)	[10]
$LaInO_3$	800 ºC, 0.7 h^{-1}, CH_4/O_2 = 5	15	54 (S)	[11]
$La_{0.9}Ba_{0.1}InO_{3-\delta}$	800 ºC, 0.7 h^{-1}, CH_4/O_2 = 5	22	59 (S)	[11]
$La_{0.6}Ba_{0.4}InO_{3-\delta}$	800 ºC, 0.7 h^{-1}, CH_4/O_2 = 5	21	61 (S)	[11]

[1] COLMENARES, M. G., Simon, U., Yildiz, M., Arndt, S., Schomaecker, R., Thomas, A., Goerke, O. Oxidative coupling of methane on the Na2WO4-MnxOy catalyst: COK-12 as an inexpensive alternative to SBA-15. Catalysis Communications, v. 85, p. 75-78, 2016.

[2] ELKINS, Trenton, W. Neumann, B., Bäumer, M., Hagelin-Weaver, H. E.. Effects of Li Doping on MgO-Supported Sm2O3 and TbO x Catalysts in the Oxidative Coupling of Methane. ACS Catalysis, v. 4, n. 6, p. 1972-1990, 2014.

[3] YILDIZ, M. Y., Simon, U., Kailasam, K., Goerke, O., Rosowski, F., Arndt, S. Enhanced catalytic performance of Mn x O y–Na 2 WO 4/SiO 2 for the oxidative coupling of methane using an ordered mesoporous silica support. Chemical Communications, v. 50, n. 92, p. 14440-14442, 2014.

[4] ASEEM, A. Jeba, G. G., Conato, M. T., Rimer, J. D.,Harold, M. P. Oxidative coupling of methane over mixed metal oxide catalysts: Steady state multiplicity and catalyst durability. Chemical Engineering Journal, v. 331, p. 132-143, 2018.

[5] RAOUF, Fereshteh; TAGHIZADEH, Majid; YOUSEFI, Mohammad. Influence of CaO–ZnO supplementation as a secondary catalytic bed on the oxidative coupling of methane. Reaction Kinetics, Mechanisms and Catalysis, v. 112, n. 1, p. 227-240, 2014.

[6] LEE, Jong Yeol et al. Scaled-up production of C2 hydrocarbons by the oxidative coupling of methane over pelletized Na2WO4/Mn/SiO2 catalysts: Observing hot spots for the selective process. Fuel, v. 106, p. 851-857, 2013.

[7] GHOSE, Ranjita; HWANG, Hyun Tae; VARMA, Arvind. Oxidative coupling of methane using catalysts synthesized by solution combustion method: Catalyst optimization and kinetic studies. Applied Catalysis A: General, v. 472, p. 39-46, 2014.

[8] OSHIMA, Kazumasa, Tanaka, K., Yabe, T., Kikuchi, E., & Sekine, Y.. Oxidative coupling of methane using carbon dioxide in an electric field over La–ZrO2 catalyst at low external temperature. Fuel, v. 107, p. 879-881, 2013.

[9] WANG, Huan, Schmack, R., Paul, B., Albrecht, M., Sokolov, S., Rümmler, S., Kraehnert, R.. Porous silicon carbide as a support for Mn/Na/W/SiC catalyst in the oxidative coupling of methane. Applied Catalysis A: General, v. 537, p. 33-39, 2017.

[10] XU, Junwei Zhang, Y., Xu, X., Fang, X., Xi, R., Liu, Y., Wang, X. Constructing La2B2O7 (B= Ti, Zr, Ce) compounds with three typical crystalline phases for the oxidative coupling of methane: the effect of phase structures, superoxide anions, and alkalinity on the reactivity. ACS Catalysis, v. 9, n. 5, p. 4030-4045, 2019.
[11] OSHIMA, Kazumasa; SHINAGAWA, Tatsuya; SEKINE, Yasushi. Methane conversion assisted by plasma or electric field. Journal of the Japan Petroleum Institute, v. 56, n. 1, p. 11-21, 2013.

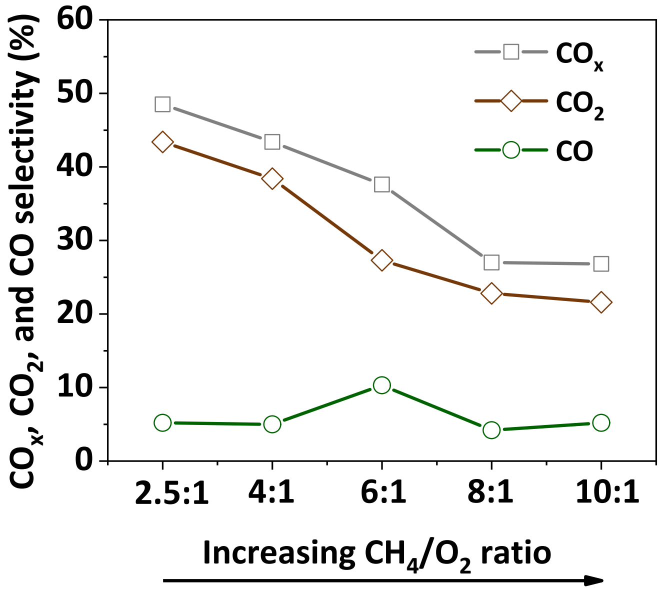

Figure 9S. CO_x (CO_2+CO), CO_2, and CO selectivities in the OCM reaction performed over $La_2(Ce_{0.6}Mg_{0.4})_2O_{7-\delta}$, varying the CH_4/O_2 ratio. Reaction conditions: 200 mg catalyst, WHSV = 18,000 $mL.h^{-1}.g_{cat}^{-1}$, 800 ºC.

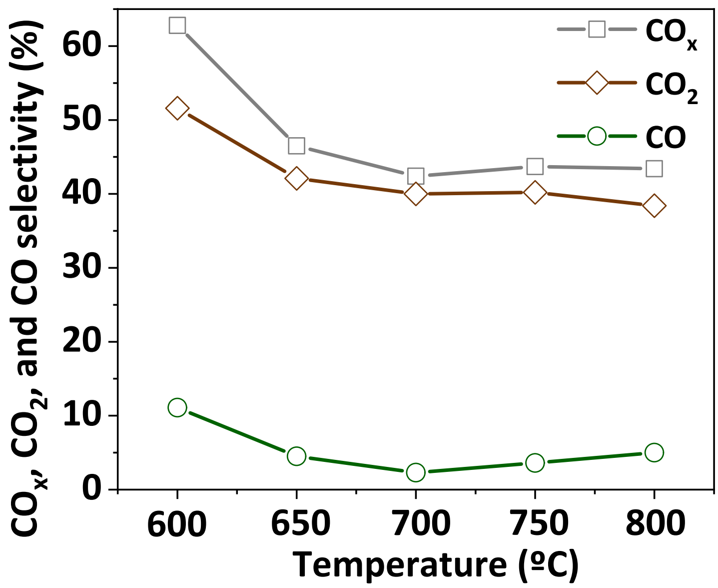

Figure 10S. CO_x (CO_2+CO), CO_2, and CO selectivities in the OCM reaction performed over $La_2(Ce_{0.6}Mg_{0.4})_2O_{7-\delta}$, varying the temperature. Reaction conditions: 200 mg catalyst, WHSV = 18,000 $mL.h^{-1}.g_{cat}^{-1}$.

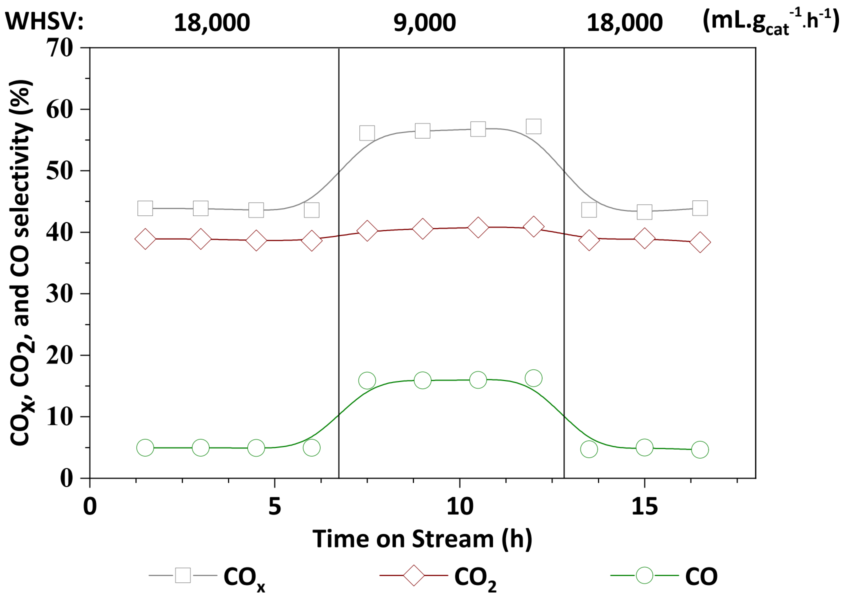

Figure 11S. CO_x (CO_2+CO), CO_2, and CO selectivities in the OCM reaction performed over the $La_2(Ce_{0.6}Mg_{0.4})_2O_{7-\delta}$ catalyst (350 mg), varying the WHSV.

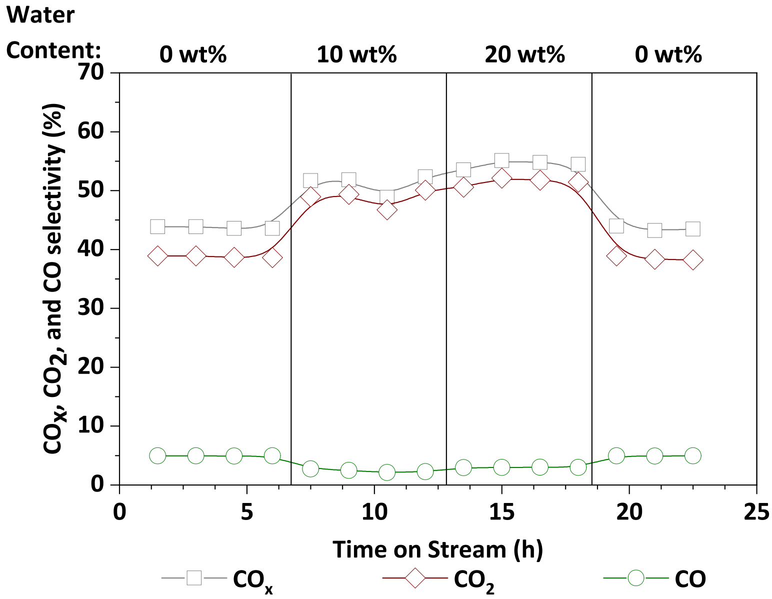

Figure 12S. CO_x (CO_2+CO), CO_2, and CO selectivities in the OCM reaction performed over the $La_2(Ce_{0.6}Mg_{0.4})_2O_{7-\delta}$ catalyst, varying the amount of water in the feed of 0 wt.% (4 CH_4: 1 O_2: 4 N_2), 10 wt.% (4 CH_4: 1 O_2: 4 N_2: 1 H_2O) and 20 wt.% (4 CH_4: 1 O_2: 4 N_2: 2.25 H_2O). Reaction conditions: 200 mg catalyst, 800 ºC, WHSV = 18,000 $mL.h^{-1}.g_{cat}^{-1}$.